Interferometric Synthetic Aperture Radar Detection and Estimation Based 3D Image Reconstruction

Christian D. Austin and Randolph L. Moses

The Ohio State University
Department of Electrical and Computer Engineering
2015 Neil Avenue, Columbus, OH 43210

ABSTRACT

This paper explores three-dimensional (3D) interferometric synthetic aperture radar (IFSAR) image reconstruction when multiple scattering centers and noise are present in a radar resolution cell. We introduce an IFSAR scattering model that accounts for both multiple scattering centers and noise. The problem of 3D image reconstruction is then posed as a multiple hypothesis detection and estimation problem; resolution cells containing a single scattering center are detected and the 3D location of these cells' pixels are estimated; all other pixels are rejected from the image. Detection and estimation statistics are derived using the multiple scattering center IFSAR model. A 3D image reconstruction algorithm using these statistics is then presented, and its performance is evaluated for a 3D reconstruction of a backhoe from noisy IFSAR data.

Keywords: synthetic aperture radar, radar imaging, interferometric SAR, three-dimensional reconstruction, detection, estimation

1. INTRODUCTION

Interferometric synthetic aperture radar processing is a method of reconstructing three-dimensional (3D) images using two-dimensional (2D) synthetic aperture radar (SAR) data from two closely spaced elevation angles. The phase difference between corresponding pixels from the two elevation angle images encode height information.[1–3] 3D images can also be formed using other methods, such as 3D SAR. This form of imaging typically utilizes SAR images at >2 elevation angles.[4] IFSAR reconstruction is advantageous from both a processing and data collection standpoint; less data needs to be processed and data collection is only necessary at two elevations angles. Furthermore, since these elevations are closely spaced, it is possible to collect both measurements using two radars on a single aircraft, making single pass data collection possible.

Two sources of error in height estimation from IFSAR imagery are noise and multiple scattering components in a resolution cell. The traditional IFSAR phase difference height estimator assumes that there is only one scattering center in a radar resolution cell. When there is more than one strong scattering center in a radar resolution cell, height estimation may be erroneous. Furthermore, spurious height estimates will result from resolution cells containing only noise, degrading image quality. Image noise may be attributed to clutter, thermal noise, layover, or some other unknown parameter in the radar imaging system or scene.

In a recent paper, the authors investigated 3D IFSAR image reconstruction of scenes with two scattering centers in a resolution cell and no noise.[5] Using geometric arguments on a noiseless two scattering center model, a pixel magnitude ratio statistic for detecting the presence of two scattering centers was proposed. A threshold test on this statistic together with one on image pixel magnitude was used in a 3D image reconstruction algorithm. Thresholds on each statistic were tuned to meet a desired level of average scene height error or visual reconstruction performance.

This paper extends previous 3D IFSAR reconstruction work to image scenes with an arbitrary number of scattering centers in a resolution cell (not just 1 or 2) and also models image noise. The problem of 3D IFSAR image reconstruction is posed as a multiple hypothesis detection and estimation problem, and a 3D IFSAR image reconstruction algorithm is developed in this framework. The proposed algorithm turns out to be very similar to the algorithm derived for image reconstruction with two scattering centers and no noise,[5] although each was developed under different assumptions and models.

We introduce a ternary hypothesis model for multiple scattering centers in a resolution cell with noise and classify resolution cells according to the number of scattering centers in the cell. The three hypotheses are zero (H_0) one (H_1) and more than one (H_2) scattering center in a resolution cell. From this hypothesis model, decision statistics for detecting each hypothesis are derived. These statistics are used together with a height estimator to form a multistage detection and estimation algorithm. The first stage of the algorithm detects the number of scattering centers in a resolution cell and consists of two binary hypothesis detectors, one for distinguishing between noise and signal (H_0 vs. $H_1 \cup H_2$) and the other for distinguishing between >1 scattering center and one scattering center or noise (H_2 vs. $H_0 \cup H_1$). The second stage consists of the traditional IFSAR phase difference height estimator. If the first stage detects one scattering center in a radar resolution cell, the data is retained and sent to the second stage for height estimation; otherwise it is discarded.

Image reconstruction performance of the proposed IFSAR algorithm is determined by thresholds on each binary test statistic in the detection stage and on the level of noise in a scene. The performance of each algorithm is assessed in reconstructing a 3D image of a construction backhoe using SAR data generated from the XPatchT scattering simulation software under different noise levels.

2. IFSAR RESOLUTION CELL MODEL

First, we present the IFSAR resolution cell multiple scattering center model that is used in subsequent analysis. We begin by giving an overview of the IFSAR imaging equations and then discuss why a multiple scattering center model is needed. A multiple scattering center model is then presented and used in a ternary hypothesis classification of resolution cells with 0, 1, or >1 scattering center in a resolution cell.

2.1. IFSAR Imaging Equations

In the following discussion, we assume that two SAR images are formed at two closely-spaced elevations angles, Ψ_1 and Ψ_2, with respect to a common slant plane at elevation angle Ψ_s. The elevation angles are closely spaced in the sense that $|\Psi_i - \Psi_s| \ll 1$ $(i = 1, 2)$ so that $\sin(\Psi_i - \Psi_s) \approx \Psi_i - \Psi_s$ and $\cos(\Psi_i - \Psi_s) \approx 1$. In the following discussion, slant plane coordinates are implied unless stated otherwise, and images formed at elevation angle Ψ_i for $i = 1, 2$ are denoted as $s_i(x, y)$.

SAR processing generates a 2D grid of discrete samples of the object being imaged. In the following discussion, a discrete sample of the image at location (x_k, y_l) on the slant plane will be denoted as an image pixel, and a resolution cell corresponding to an image pixel centered at some point (x_k, y_l) will be defined as

$$\mathbf{C_{k,l}} = \left\{ (x, y, z) : x_k - \frac{x_{\text{res}}}{2} \le x \le x_k + \frac{x_{\text{res}}}{2},\ y_l - \frac{y_{\text{res}}}{2} \le y \le y_l + \frac{y_{\text{res}}}{2},\ \frac{-z_{\max}}{2} \le z \le \frac{z_{\max}}{2} \right\}, \tag{1}$$

where x_{res} and y_{res} are the resolutions in the x and y dimensions, respectively, and $z_{\max}$ is the maximum height range of the scene, which is often defined from the beamwidth of the radar.

In traditional IFSAR processing, when there is one scattering center in a resolution cell at height $h(x, y)$, the image pixel response at elevation angle Ψ_i, $s_i(x, y)$, at image location (x, y) is given by[1]

$$\begin{aligned} s_i(x, y) &\approx \text{sinc}_{\Delta X, \Delta Y}(x, y) \otimes \left[r(x, y) e^{-j4\pi \sin(\Psi_i - \Psi_s) h(x,y)/\lambda_c} e^{-j4\pi \cos(\Psi_i - \Psi_s) y/\lambda_c} \right] \\ \text{sinc}_{\Delta X, \Delta Y}(x, y) &= \Delta X \Delta Y \text{sinc}\left(\tfrac{x \Delta X}{2\pi}\right) \text{sinc}\left(\tfrac{y \Delta Y}{2\pi}\right), \end{aligned} \tag{2}$$

where λ_c is the wavelength of the radar center frequency, ΔX and ΔY are the width of the support of the data collection in the crossrange and downrange Fourier dimensions X and Y, and $r(x, y)$ is the reflectivity function of the scene. A pixel at location (x_k, y_l) will be denoted as $s_i(x_k, y_l)$.

When there is one scattering center in a resolution cell, (2) can be used to derive a z-coordinate height estimate of this scattering center orthogonal to the slant plane; the height estimate can be calculated as the phase difference between image pixels[1]:

$$\hat{z} = \frac{1}{k_I} \arg(s_2 s_1^*), \tag{3}$$

where $k_I = \frac{4\pi\Delta\Psi}{\lambda_c}$ is the height-to-phase scaling factor and s_i is used to denote the image pixel value under consideration, $s_i(x_k, y_l)$, for simplicity of notation. The mapping from phase difference to height is ambiguous if the phase difference exceeds 2π. Hence, we define the unambiguous IFSAR height interval as $2\pi/k_I$.

For an imaging scene where the height varies slowly with respect to SAR image resolution, such as in topographic mapping, the single-pixel height estimator (3) can be modified to provide some averaging over multiple pixels.[1] However, in applications such as 3D target reconstruction, height of the imaging scene may vary quickly with respect to image resolution; so, we use single pixel height estimates to avoid bias due to smoothing.

When more than one scattering center lies within a resolution cell or when the cell contains only noise, height estimation using (3) may result in erroneous height estimates. In the following sections, we propose a SAR resolution cell model that incorporates the possibility of multiple scattering centers and noise in a resolution cell and develop an IFSAR reconstruction algorithm based on this model.

2.2. Multiple Scattering Center Model

Using the IFSAR equations from the previous section, we present a scattering center model for resolution cells with multiple scattering centers in a resolution cell and noise. Before introducing this model, we justify the need to consider an arbitrary number of scattering centers in a resolution cell. If there is a negligible number of resolution cells with >1 scattering centers, a model using (2) with the addition of noise should model an image scene well, and detecting resolution cells with >1 scattering centers would be unnecessary. However, 3D scattering analysis of ground targets suggests otherwise.

To illustrate that there is in fact a non-negligible number of resolution cells with >1 scattering centers for a complex target, we present ground truth results from an XPatchT model of a construction backhoe. Ground truth data is generated by the ray-tracing engine in XPatch and is defined as a list of all of the scattering center 3D locations quantized to high spatial resolution and magnitudes of the object being imaged, regardless of the image resolution.[6] This means that with ground truth data, information about each of the scattering centers in a resolution cell is available separately.

A histogram of the number of scattering centers in a SAR image resolution cell for an image formed at an azimuth angle of 85° and elevation angle of 30° is shown in Figure 1. The histogram is generated using XpatchT backhoe ground truth data from resolution cells defined by (1) for an X-band radar with a resolution of approximately 1.5 in. $\times$ 1.5 in. over a scene of approximately 20 m. $\times$ 20 m.. The scene consisted of a backhoe in free space, meaning that the backhoe was the only object in the scene with scattering centers. Most of the resolution cells in the scene do not contain scattering centers, and are omitted from the histogram in Figure 1, which only displays resolution cells with $\geq$1 scattering center. This figure shows that the number of resolution cells with >1 scattering centers is not negligible compared to resolution cells with one scattering center. Furthermore, the response of resolution cells with >1 scattering centers are not necessarily dominated by the response of one strong scattering center, as implied by Figure 2 and the following discussion of interfering scatter centers. This example suggests that a model that incorporates only one scattering center with noise will not model a complex image scene, like the backhoe scene, well.

Letting the image formation slant plane elevation be equal to the lowest data collection elevation angle, $\Psi_1 = \Psi_s$, and using (2), an image pixel for a resolution cell with one scattering center at elevation Ψ_i can be written as[1]

$$Ae^{j\alpha}e^{j(i-1)k_I z}, \tag{4}$$

where $A \in \mathbb{R}^+$ is the magnitude of the image pixel, which is constant over small elevation changes; $\alpha \in [-\pi, \pi)$ is a constant phase factor; $z \in \mathbb{R}$ is the height of the pixel in meters above the image formation slant plane, and k_I is the height-to-phase scaling factor defined previously.

The complex image pixel value of a resolution cell with multiple scattering centers is modeled as the coherent sum of individual scattering center responses in the resolution cell. The multiple scattering center model for a

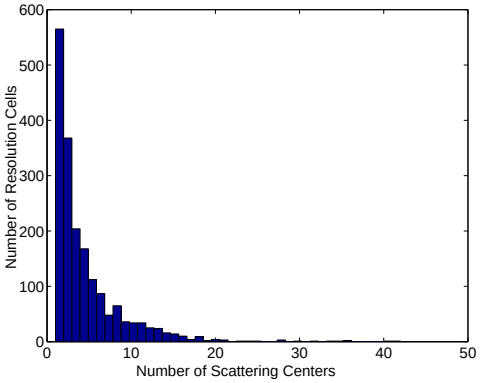

Figure 1. Histograms of the number of scattering centers in 1.5 in. × 1.5 in. resolution cells for an image formed at an azimuth angle of 85° and an elevation angle of 30°. Only resolution cells with ≥1 scattering center are shown.

resolution cell is the resulting complex image pixel value of the resolution cell at each elevation angle Ψ_i with additive noise:

$$\bar{\mathbf{S}}_N \triangleq \begin{bmatrix} \bar{s}_1 \\ \bar{s}_2 \end{bmatrix} = \sum_{m=1}^{M} A_m \underbrace{\begin{bmatrix} e^{j\alpha_m} \\ e^{j(\alpha_m + k_I z_m)} \end{bmatrix}}_{\mathbf{M}_m} + \underbrace{\begin{bmatrix} n_1 \\ n_2 \end{bmatrix}}_{\mathbf{N}} = A_1\mathbf{M}_1 + \sum_{m=2}^{M} A_m\mathbf{M}_m + \mathbf{N}$$

$$= A_1\mathbf{M}_1 + \bar{\mathbf{M}}_I + \mathbf{N}. \tag{5}$$

Here, the (x_k, y_l) coordinates are omitted for brevity. The vector $\mathbf{S}_N \in \mathbb{C}^2$ consists of noisy pixel values, $\bar{s}_i$, at elevation angle Ψ_i. The terms A_m, α_m, and z_m are the terms A, α, and z in (4) for the m^{th} scattering center in the resolution cell. Noise is introduced in the $\mathbf{N}$ vector with noise components n_i at elevation angle Ψ_i that are independent identically distributed (*iid*) with complex Gaussian distribution $C\mathcal{N}(\mathbf{0}, \sigma_n^2\mathbf{I})$ and known variance σ_n^2. Magnitude values A_n are ordered such that $A_n > A_m$ if $n < m$, making A_1 the largest magnitude. The scattering center associated with the largest magnitude, A_1 is denoted as the dominant scattering center in the resolution cell and all others are denoted as interfering scattering terms. Accordingly, vectors $A_1\mathbf{M}_1$ and $\bar{\mathbf{M}}_I$ are denoted as the dominant scattering and interfering scattering vectors, respectively.

Without loss of generality, we represent the interference vector, which is the coherent sum of interfering scattering centers, as a vector in $\mathbb{C}^2$ with arbitrary complex components:

$$\bar{\mathbf{M}}_I \triangleq \begin{bmatrix} \bar{A}_{I_1} e^{j\bar{\theta}_1} \\ \bar{A}_{I_2} e^{j\bar{\theta}_2} \end{bmatrix}. \tag{6}$$

The variables $\bar{A}_{I_i} \in \mathbb{R}^+$ are interference magnitude values at elevation angle Ψ_i, and the $\bar{\theta}_i \in [-\pi, \pi]$ variables are interference phase values at elevation angle Ψ_i.

The multiple scattering center model in (5), with interfering scattering given by (6), is described by the parameter vector

$$\Theta = \left(A_1, \bar{A}_{I_1}, \bar{A}_{I_2}, z_1 k_I, \alpha_1, \bar{\theta}_1, \bar{\theta}_2\right), \tag{7}$$

where the parameters are deterministic and unknown. It is desirable to establish a random interfering scattering vector, (6), for the purpose of eliminating unknown nuisance parameters from the statistical tests developed in Section 3.

XPatchT backhoe ground truth data has been used to develop a random interfering scattering model.[7] This data indicates that given the magnitude of the dominant scattering center, A_1, the magnitude of the coherent sum of interfering scattering, $\bar{A}_{I_i}$, is well-modeled as Rayleigh distributed with a Rayleigh parameter that is linearly proportional to A_1. Figure 2(a) shows an example of the conditional Rayleigh distribution of $\bar{A}_{I_i}$ fit to the ground truth data using a maximum-likelihood estimate of the Rayleigh parameter, and Figure 2(b) shows

the linear relationship between the magnitude of the dominant scattering center using a least squares fit to the Rayleigh parameter estimates. The slope of the least squares fit is denoted as σ_I^2 and is approximately 0.78 for this data.

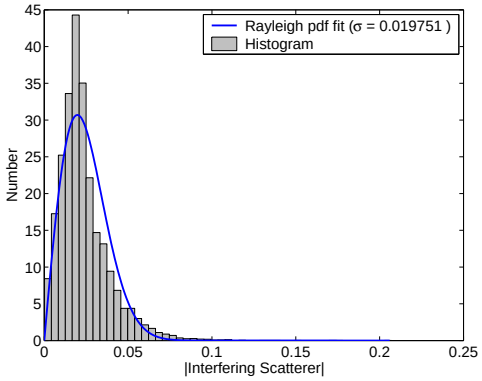

(a) Histogram of $\bar{A}_{I_1}$ given $0.02 < A_1 < 0.03$ and superimposed Rayleigh distribution with parameter σ.

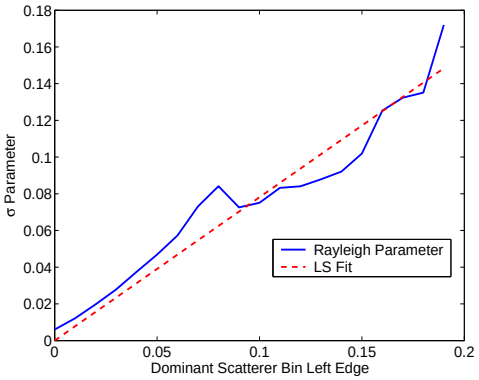

(b) Rayleigh parameter σ as a function of A_1 for Rayleigh distributions fit to the backhoe ground truth data $\bar{A}_{I_1}$ given $\tau_{min} < A_1 < \tau_{max}$, where $\tau_{max} - \tau_{min} = 0.01$.

Figure 2. Conditional distribution of interfering scattering magnitude and linear relationship between the Rayleigh parameter of $\bar{A}_{I_1}$ and A_1.

Furthermore, the distribution of the interfering scattering phase $\bar{\theta}_i$, conditioned on the dominant scattering phase, can be approximated as uniform in $[-\pi,\ \pi]$.[7] Under the assumption that the interference at elevation angle Ψ_i, $\bar{A}_{I_1}e^{j\bar{\theta}_1}$, is random and *iid* for each $i = 1, 2$ and that magnitudes of the dominant and interfering scattering magnitude, A_1 and $\bar{A}_{I_i}$ respectively, are statistically independent of each of the dominant and interfering scattering phases, $z_1 k_I$, α_1, $\bar{\theta}_1$, and $\bar{\theta}_2$, a distribution on the interfering scattering can be derived. We let $\bar{\mathbf{M}}_I \stackrel{\triangle}{=} [m_{I_1},\ m_{I_2}]^T$ denote the interference vector when interference is modeled randomly. The terms m_{I_i} for $i = 1, 2$ denote the *iid* complex random interfering scattering at elevation Ψ_i, and the distribution of $\bar{\mathbf{M}}_I$ is[7]

$$\bar{\mathbf{M}}_I = \begin{bmatrix} m_{I_1} \\ m_{I_2} \end{bmatrix} \sim C\mathcal{N}(\mathbf{0}, \sigma_I^2 A_1^2 \mathbf{I}), \tag{8}$$

given (deterministic) A_1, $z_1 k_I$, and α_1.

In the following sections, the multiple scattering center model in (5) is used in classifying resolution cells in terms of a multiple hypothesis model. This model, using both deterministic unknown interfering scattering in (6) and the random interfering scattering characterized by (8), is used in developing statistics for 3D IFSAR image reconstruction.

2.3. Ternary Hypothesis Model

The number of scattering centers in a resolution cell can be classified as 0, 1, or >1, giving a ternary classification of a resolution cell. In this section, we develop a ternary hypothesis model of the resolution cells in an imaging scene based on the number of scattering centers in a resolution cell.

Using the multiple scattering center model in (5), the following ternary hypothesis model can be used to classify resolution cells in an image scene:

$$\begin{aligned} H_0 &: \bar{\mathbf{S}}_N = \mathbf{N} \\ H_1 &: \bar{\mathbf{S}}_N = A_1\mathbf{M}_1 + \mathbf{N} \\ H_2 &: \bar{\mathbf{S}}_N = A_1\mathbf{M}_1 + \bar{\mathbf{M}}_I + \mathbf{N}. \end{aligned} \tag{9}$$

Hypothesis H_0 classifies a resolution cell with zero scattering centers (only noise). In this case, all magnitude parameters in the multiple hypothesis model, A_1, and $\bar{A}_{I_i}$, are zero. A resolution cell with one scattering center is classified as hypothesis H_1, where all interference magnitudes in the multiple scattering center model, $\bar{A}_{I_i}$, are zero and A_1 is non-zero; H_2 is the hypothesis that classifies resolution cells with >1 scattering center, and is represented by the multiple scattering center model with non-zero A_1 and at least one non-zero $\bar{A}_{I_i}$ in (6).

Since the noise parameter, $\mathbf{N}$, is distributed as $C\mathcal{N}(\mathbf{0}, \sigma_n^2\mathbf{I})$ with known variance σ_n^2, and the dominant scattering center parameters, A_1, α_1, and z_1 are deterministic and unknown, the pixel distributions under hypothesis H_0 and H_1 are complex Gaussian, since they are affine transformations of Gaussians. The distribution under H_0 is $C\mathcal{N}(\mathbf{0}, \sigma_n^2\mathbf{I})$ and the distribution under H_1 is $C\mathcal{N}(A_1\mathbf{M}_1, \sigma_n^2\mathbf{I})$. If we make no assumptions about the distribution of the interfering scattering and specifying it as a deterministic and unknown vector given by (6), the distribution under H_2 is

$$C\mathcal{N}(A_1\mathbf{M}_1 + \bar{\mathbf{M}}_I, \sigma_n^2\mathbf{I}). \tag{10}$$

On the other hand, if we assume that the interference is random and specified by the distribution in (8), the distribution under H_2 is

$$C\mathcal{N}(A_1\mathbf{M}_1, \left(A_1^2\sigma_I^2 + \sigma_n^2\right)\mathbf{I}). \tag{11}$$

3. DETECTION TEST STATISTICS

In this section, we use the ternary hypothesis model (9) to develop binary hypothesis test statistics for distinguishing between the number of scattering centers in a resolution cell. These tests are used in the detection stage of the proposed image reconstruction algorithm. In particular, binary tests for testing noise versus no noise and ≤ 1 scattering center versus >1 scattering center are discussed. Tests that are invariant or nearly invariant to the unknown parameters in the ternary hypothesis model and that have constant false alarm rates (CFAR) or are nearly CFAR are desirable.

3.1. Generalized Likelihood Ratio Test (GLRT) for Noise Detection

A GLRT is a likelihood ratio test with unknown deterministic parameters replaced by their maximum-likelihood (ML) ratio estimates. From the ternary hypothesis model, the noise only hypothesis is H_0, and the scattering center plus noise case is that of ≥ 1 scattering centers in a resolution cell, $H_1 \cup H_2$. In deriving a statistic for noise detection, the interfering scattering vector, $\bar{\mathbf{M}}_I$, is modeled with deterministic and unknown parameters and is given by (6); No distributions are imposed on the parameters. Since hypothesis H_1 is nested in H_2, meaning that H_1 is a particular case of H_2 with the interference magnitudes, $\bar{A}_{I_i} = 0$, we use a GLRT of H_0 versus H_2 for testing noise-only resolution cells versus resolution cells with ≥ 1 scattering center.

Finding the ML estimate of the parameters Θ in (7), substituting these values into the distribution of H_2 given by (10) and taking the likelihood ratio of the resulting function and the distribution of H_0, gives a binary hypothesis test for testing H_0 versus H_2. This test is[7]

$$m_1(\bar{\mathbf{S}}_N) \stackrel{\triangle}{=} \|\bar{s}_1\|^2 + \|\bar{s}_2\|^2 \underset{H_0}{\overset{H_2}{\gtrless}} \tau_1, \tag{12}$$

where τ_1 is a threshold set to meet a desired false alarm level of falsely rejecting H_0. Choosing H_2 in this test is understood to mean choosing $H_1 \cup H_2$ because of hypothesis nesting. The m_1 test itself is invariant to the unknown model parameters, and is a CFAR test, since the distribution of m_1 under H_0 is not a function of unknown parameters. This test can be interpreted as an energy detector, which measures the energy in the pixels, $\bar{s}_i$, to determine if the resolution cell contains a scattering signal or only noise.

3.2. Near Uniformly Most Powerful Invariant (UMPI) Test for Multiple Scattering Center Detection

In this section, we introduce a statistic for discriminating between resolution cells with ≤ 1 scattering center or >1 scattering center. A binary hypothesis test for discriminating between these two cases is one that tests $H_0 \cup H_1$ versus H_2. The hypothesis H_0 is a special case of H_1 with $A_1 = 0$; hence, it is nested in the hypothesis H_1. Thus, we use a binary test for testing H_1 versus H_2 as a test of ≤ 1 versus >1 scattering center.

A GLRT-based test using the ternary hypothesis scattering center model (7) and deterministic unknown interference parameters results in a test statistic that is free of unknown parameters, but the false alarm, which is defined as the probability of falsely rejecting H_2, will be a function of unknown model parameters, and the test will not be CFAR or even nearly CFAR.[7]

Instead, we derive a near UMPI test. A UMPI test is a binary hypothesis test that is the most powerful test out of all tests that are invariant to a group of transformations on the data. Invariance to a group of transformations $\mathcal{G}$ means that if $m(\cdot)$ is the binary test statistic and $T(\cdot)$ is from $\mathcal{G}$, then $m(T(\mathbf{x})) = m(\mathbf{x})$. This test is invariant to unknown model parameters and is CFAR. Finding a UMPI test consists of first defining a group of data transformations $\mathcal{G}$ that operate on the distribution of the data only through the parameters of the distribution, preserving the family of the distribution, and defining a maximal invariant statistic with respect to the group $\mathcal{G}$. A maximal invariant statistic m is one that is invariant to $\mathcal{G}$ and also is maximal in the sense that if $m(\mathbf{x}_1) = M(\mathbf{x}_2)$ then $\exists\ T(\mathbf{x}) \in \mathcal{G}$ such that $T(\mathbf{x}_1) = \mathbf{x}_2$. A test is defined as the likelihood ratio of m under two competing hypotheses; the test is UMPI if the false alarm is not a function of unknown parameters, meaning it is CFAR. A more detailed discussion of maximal invariant statistics can be found in the literature.[7–9]

We use the ternary hypothesis model (7) and assume random interfering scattering characterized by (8) for purposes of a near UMPI test for testing H_1 versus H_2. The group of transformations used in UMPI development is

$$\mathcal{G} \triangleq \left\{ c\mathbf{R} \triangleq c \begin{bmatrix} e^{j\phi_1} & 0 \\ 0 & e^{j\phi_2} \end{bmatrix} :\ c > 0,\ \phi_i \in [-\pi, \pi) \right\}. \tag{13}$$

This transformation operates on the data distribution through the unknown parameters A_1, α_1, and z_1 and preserves the distribution family.[7] The statistic

$$m_2(\bar{\mathbf{S}}_N) \triangleq \frac{\|\bar{s}_1\|^2 - \|\bar{s}_2\|^2}{\|\bar{s}_1\|^2 + \|\bar{s}_2\|^2} \tag{14}$$

is a maximal invariant statistic with respect to the group of data transformations $\mathcal{G}$ in (13). Using m_2, the near UMPI test of H_1 versus H_2 with false alarm defined as the probability of falsely rejecting H_2 is[7]

$$m_3(\bar{\mathbf{S}}_N) \triangleq \left| \frac{\|\bar{s}_1\|^2 - \|\bar{s}_2\|^2}{\|\bar{s}_1\|^2 + \|\bar{s}_2\|^2} \right| \underset{H_1}{\overset{H_2}{\gtrless}} \tau_3, \tag{15}$$

where τ_3 is a threshold set to meet a desired false alarm level of falsely rejecting H_2. This test is called near UMPI because, while it is not strictly UMPI because the false alarm of m_3 is a function of unknown model parameters A_1, α_1, and z_1, it is a weak function of these parameters and is nearly CFAR for H_1 resolution cells with moderate to high SNR. The signal to noise ratio (SNR) for resolution cells classified under H_1 is defined as $\frac{A_1^2}{\sigma_n^2}$. For example, in the backhoe imaging scene, with $\sigma_I^2 \approx 0.6$ as in Figure 2(b), a SNR ≥ 1.67 is sufficiently large to meet the moderate to large SNR requirement.[7] The threshold τ_3 can be set to attain a false alarm bound on this test, which is nearly constant over parameter values, given the nearly CFAR nature of the test.[7] This false alarm bound will simply be called the false alarm of the test in the following discussion.

Choosing H_1 in this test is understood to mean choosing $H_1 \cup H_0$ because of hypothesis nesting, and hence m_3 is a test for discriminating between resolution cells $\leq$1 scattering center or >1 scattering center. Lastly, we note that the assumption of at least small to moderate SNR for H_1 resolution cells be should be valid most of the time for the image reconstruction algorithm proposed in the next section. In the algorithm, H_1 resolution cells with small SNR will be discarded as noise and will not be processed by m_3.

4. DETECTION AND ESTIMATION ALGORITHM

In the previous section, we derived binary detection tests for distinguishing between the number of scattering centers in a resolution cell. In this section, we discuss the use of these tests together with the traditional IFSAR phase difference height estimator in an IFSAR 3D reconstruction algorithm. The algorithm we propose is a two stage detection and estimation algorithm. The first stage detects the number of scattering centers and the second stage estimates the height of the pixel in a resolution cell based on the decision of the detection stage.

The objective is to improve IFSAR image reconstruction by only estimating the height of pixels from resolution cells with one scattering center. The height estimate of pixels from resolution cells with zero or >1 scattering center are assumed to be erroneous and are discarded by the algorithm.

The binary tests given by (12) and (15) form the detection stage of the 3D reconstruction algorithm, and the tests will be denoted by the name of their test statistics, m_1, and m_3 respectively. Thresholds are set on each test so that each achieves a desired false alarm rate. IFSAR data from a resolution cell, $\mathbf{S}_N$, is evaluated by the the m_1 noise test first. If the test declares noise (H_0), the data from the resolution cell is discarded; if not, it is evaluated by the m_3 multiple scattering center test. If the m_3 test declares that the data is from a resolution cell with >1 scattering center (H_2), the data is discarded. A resolution cell whose data is retained by both tests is declared as H_1, a resolution cell with exactly one scattering center, and the height of the pixel in the resolution cell is estimated by the IFSAR phase difference estimator given in (3). Pixels not discarded by the algorithm have magnitude values and location coordinates in $\mathbb{R}^3$; these pixels can be used to form a 3D reconstruction of the imaged scene. We note that the IFSAR phase difference estimator is the ML estimator of the dominant scattering center height under H_1 and also under H_2 for the interfering scattering model where the interference is distributed according to (8).[7]

Figure 3 shows an example of the rejection and acceptance regions of the IFSAR reconstruction algorithm detection stage as a function of measured pixel magnitudes at elevation angle Ψ_i, s_i. In this example the threshold on m_1 and m_3 are set to $\tau_1 = 0.3$ and $\tau_3 = 0.5$ respectively. IFSAR data, $\bar{\mathbf{S}}_N$ in (5), that falls within the shaded region is retained by the detector and used to estimate the height of the corresponding resolution cell. Any data outside of this region is discarded by one of the binary tests, m_1 or m_3, and hence by the detector.

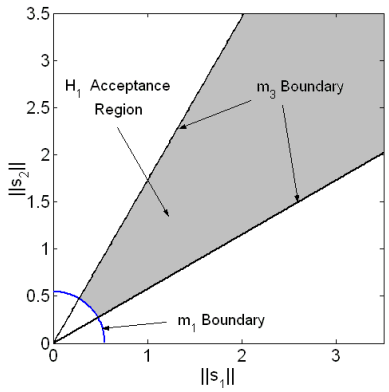

Figure 3. Acceptance and rejection regions of IFSAR reconstruction algorithm detection stage.

The quality of a 3D reconstructed image is a function of the height estimation accuracy. Figure 4 shows example IFSAR height estimation error histograms for each hypothesis of the ternary hypothesis model with height estimated by the IFSAR phase difference estimator given in (3). Height error is the difference between the actual height of the dominant scattering center in a resolution cell and the estimated height. The true height of resolution cells with no scattering centers (H_0) is taken to be zero. Each histogram is generated using the random interference model in (8) with $\sigma_I^2 = 0.6$, $\sigma_n^2 = 0.07^2$, and dominant scattering parameters distributed as $A_1 \sim \text{Ray}(\sigma_s)$, with $\sigma_s = 0.7$, $k_I z_1 \sim \mathcal{U}[-\pi,\ \pi]$, and $\alpha \sim \mathcal{U}[-\pi,\ \pi)$, where $\mathcal{U}[-\pi,\ \pi)$ denotes a uniform distribution on the interval $[-\pi,\ \pi)$ and $\text{Ray}(\sigma_s)$ denotes a Rayleigh distribution with parameter σ_s. The parameter σ_I^2 is set to 0.6 because this is approximately the value of the backhoe scene (see Figure 2(b)); the remaining parameters are set to achieve a signal to noise ratio, $\frac{\sigma_s^2}{\sigma_n^2}$, of 20dB. Figure 4 shows that H_1 resolution cells have much lower probability of large height error than resolution cells under other hypotheses. It is because of this property that the IFSAR reconstruction algorithm is designed to only use H_1 resolution cell pixels.

The false alarm rate of each binary hypothesis test in the IFSAR reconstruction algorithm detector is set by choosing an appropriate threshold on each test. Ideally, the detector would reject all resolution cells under H_0 or H_2. By lowering the false alarm rate of each binary test, the number of H_0 or H_2 resolution cells not rejected by

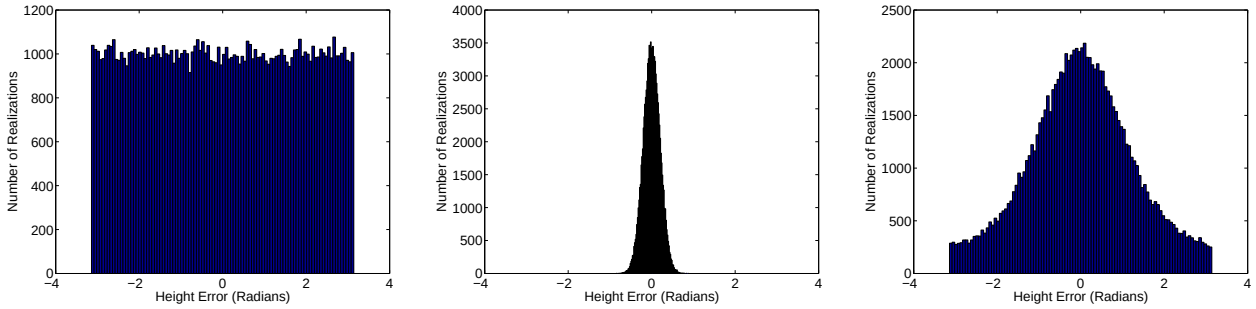

(a) Height error under H_0 for $\sigma_n^2 = 0.07^2$

(b) Height error under H_1 for $\sigma_n^2 = 0.07^2$, $A_1 \sim \text{Ray}(0.7)$, and $k_I z_1, \alpha_1 \sim \mathcal{U}[-\pi,\ \pi)$

(c) Height error under H_2 for $\sigma_n^2 = 0.07^2$, $\sigma_i^2 = 0.6$, $A_1 \sim \text{Ray}(0.7)$, and $k_I z_1, \alpha_1 \sim \mathcal{U}[-\pi,\ \pi)$

Figure 4. Histograms of height error using the $\hat{z}$ estimator under each hypothesis in the ternary hypothesis model and 100000 realizations.

the algorithm will decrease. However, decreasing the false alarm also decreases the power of the detector, and it will reject more H_1 pixels. Very low false alarm rates will result in low-quality reconstructed images because of a sparse number of pixels, and is not desirable; there is intrinsically a trade-off between image pixel sparsity and pixel height error. Figure 4 suggests that it may be appropriate to set a lower false alarm rate on m_1 than on m_3, since the probability of large height error is higher under H_0 than under H_2. Lastly, we note that the tests used in the 3D IFSAR reconstruction algorithm presented here are similar to the pixel magnitude threshold test and $\tilde{m}$ tests previously developed for two scattering centers and no noise.[5]

5. ALGORITHM PERFORMANCE

In this section, we evaluate the performance of the IFSAR 3D reconstruction detection and estimation algorithm. Performance is evaluated through 3D image reconstruction of a backhoe using XPatchT IFSAR data. We examine the 3D IFSAR reconstruction performance on a backhoe image scene under different noise levels. All backhoe IFSAR data is generated using XPatchT scattering simulation software for an X-Band radar with center frequency, $f_c = 10$GHz, and bandwidth of 4GHz; noise is added to each of the images synthetically, and VV polarization is used in image reconstruction processing.

A facet model of the backhoe that will be reconstructed is shown in Figure 5. Figures 6 and 7 show 2D SAR reconstructions, 3D IFSAR reconstructions using the proposed algorithm, and 3D pixel rejection images of the backhoe under different noise levels. 3D Images are reconstructed using data for the entire "upper hemisphere" of the backhoe image scene, with IFSAR image pairs spaced at 0.05° in elevation angle. "Upper hemisphere" means all IFSAR image data centered every 5° in azimuth angle from 0° to 355° and at elevation angles of $5n°$ and $(5n° + 0.05)°$ for $n = 0, \ldots 17$. Noise variances, σ_n^2 are set so that they are a certain decibel level below the power of the strongest pixel in the set of pixels formed by taking all pixels from SAR images formed at each aspect angle of the upper hemisphere and removing the strongest 0.01% of pixels. Removing this 0.01% of pixels removes strong outliers from the set. Figure 6 and 7 shows images formed with noise variance 30dB and 20dB below the strongest 0.01% of pixels respectively.

Figures 6(a) and 7(a) are 2D reconstructions of the backhoe at an azimuth and elevation angle pair, $(\text{azimuth}, \text{elevation})$, of $(0°, 0°)$ for noise variances 30 and 20dB below the strongest 0.01% of pixels respectively, and Figures 6(b) and 7(b) are 2D reconstructions at azimuth and elevation angle pair $(45°, 45°)$ for noise variances 30 and 20dB below the strongest 0.01% of pixels respectively. The bar next to each figure encodes the magnitude of each pixel in decibels with respect to the maximum pixel magnitude of the SAR images formed at azimuth and elevation aspect angles of $(0°, 0°)$ and $(45°, 45°)$. These images show how the level of noise compares with image pixel strength; images formed with a higher noise level, 20dB below the top 0.01% of scattering magnitude, blend into the background more than images at 30dB below.

Figure 5. Facet model of backhoe.

Examples of 3D IFSAR image reconstructions using the IFSAR detection and estimation algorithm proposed in Section 4 are shown in Figures 6(c) and 7(c) for noise variances 30 and 20dB below the strongest 0.01% of pixels respectively. In the following discussion, we specify detector settings in terms of the binary hypothesis thresholds τ_1 and τ_3, each of which correspond to false alarm rates on m_1 and m_3. A discussion of false alarm rate calculation from thresholds can be found in the reference by Austin.[7]

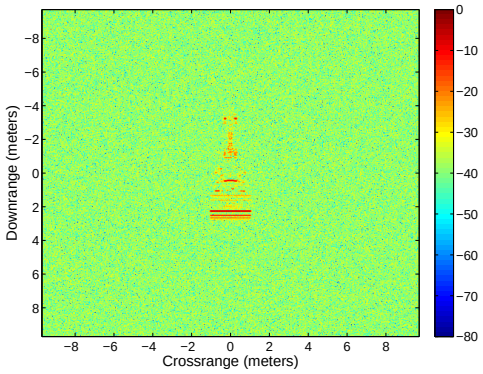

(a) 2D backhoe reconstruction at azimuth = 0°, elevation = 0°.

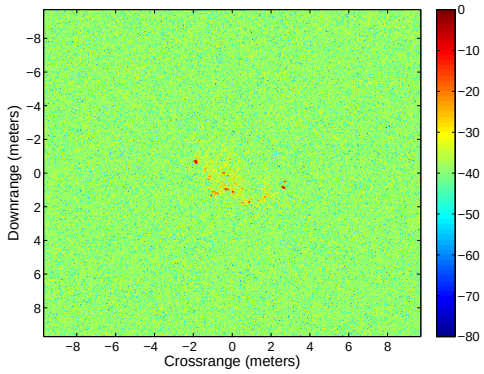

(b) 2D backhoe reconstruction at azimuth = 45°, elevation = 45°.

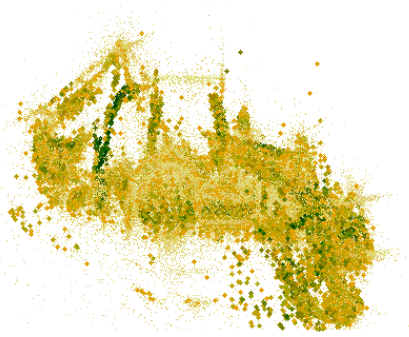

(c) 3D reconstruction of backhoe using "upper hemisphere" of IFSAR data, $\tau_1 = 0.11$ and $\tau_3 = 0.1$.

(d) Rejection image of 3D reconstructed backhoe. Only pixels rejected by m_3 are plotted.

Figure 6. 2D and 3D IFSAR algorithm based reconstructed backhoe images with a noise variance of $\sigma_n^2 = 0.00039$ (30 dB below the strongest 0.01% of pixels in the scene)

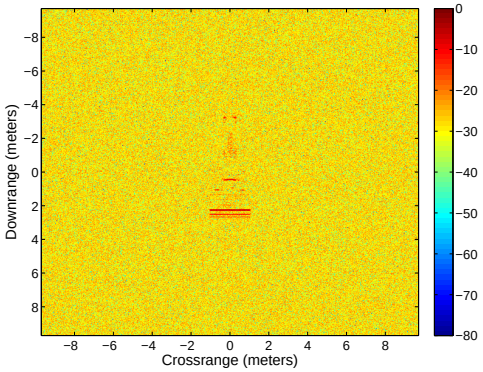

(a) 2D backhoe reconstruction at azimuth = 0°, elevation = 0°.

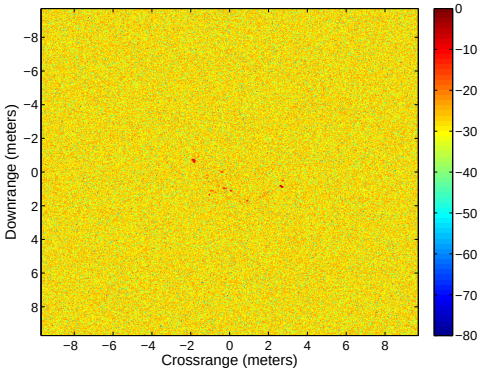

(b) 2D backhoe reconstruction at azimuth = 45°, elevation = 45°.

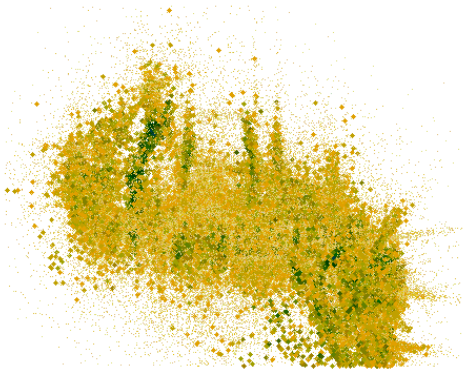

(c) 3D reconstruction of backhoe using "upper hemisphere" of IFSAR data, $\tau_1 = 0.15$ and $\tau_3 = 0.4$.

(d) Rejection image of 3D reconstructed backhoe. Only pixels rejected by m_3 are plotted.

Figure 7. 2D and 3D IFSAR algorithm based reconstructed backhoe images with a noise variance of $\sigma_n^2 = 0.0039$ (20 dB below the strongest 0.01% of pixels in the scene)

The image in Figure 6(c) is generated using detector threshold settings of $\tau_1 = 0.11$ and $\tau_3 = 0.1$, and the image in Figure 7(c) is generated with threshold settings of $\tau_1 = 0.15$ and $\tau_3 = 0.4$. Larger darker pixels (dark green) in the image correspond to pixels with larger magnitude; smaller magnitude pixels are smaller in size and become lighter (light yellow). Threshold settings were chosen manually to achieve a trade-off between images with a large number of pixels that do not lie close to the backhoe surface and sparse images. Different threshold settings will result in different "quality" images, where "quality" depends on the application. Figure 6(c) appears visually sharper than Figure 7(c); as may be expected, this can be attributed to the larger noise variance in the latter figure. Rejection images of the 3D reconstructed backhoe images in Figures 6(c) and 6(c) are presented in Figures 6(d) and 7(d) respectively. These images are the pixels rejected by the m_3 test in the detector, meaning that the m_3 detector classified them as originating from resolution cells with >1 scattering center. Many pixels that do not lay close to surface of the backhoe, clouding the image, are shown in the rejection images. Rejection images of the m_1 test are not shown because there are a large number of pixels in these images, and the pixels appear as a cloud around the backhoe with no structure.

6. CONCLUSION

A detection and estimation based 3D IFSAR reconstruction algorithm for resolution cells with an arbitrary number of scattering centers and noise was developed in this paper. We argued, using XPatchT backhoe data, that for complex image scenes, such as the backhoe scene, there are many resolution cells with >1 scattering

center. Furthermore, we showed that it is not, in general, valid to assume only one dominant scattering center in these resolution cells. A resolution cell model with noise was proposed to account for multiple scattering centers. This model was used to develop a ternary hypothesis model which classifies resolution cells in an image scene by the number of scattering centers they contain; XPatchT data was also used in conjunction with the multiple scattering model to describe interfering scattering randomly. Using the ternary hypothesis model, two binary hypothesis tests were developed: a GLRT test for detecting resolution cells with only noise and a near UMPI test for detecting resolution cells with >1 scattering center. We then proposed the two stage detection and estimation 3D IFSAR reconstruction algorithm. The GLRT and near UMPI binary tests were used in the detection stage, which detects resolution cells with only 1 scattering center; the estimation stage uses the standard IFSAR phase difference estimator to estimate the heights of resolution cells declared to have one scattering center by the detection stage.

Performance of the 3D IFSAR reconstruction algorithm was evaluated on XPatchT generated IFSAR data. Reconstructed backhoe images were formed at different noise levels, a low to moderate and higher noise level. In both cases, the structure of the backhoe was visible in reconstructed images, but the lower noise level image was sharper. The IFSAR reconstruction algorithm appears to eliminate may pixels that are not close to the surface of the backhoe and visually appears to be effective in 3D reconstruction of image scenes with an arbitrary number of scattering centers and noise.

ACKNOWLEDGMENTS

The authors would like to thank Rajan Bhalla of SAIC for providing XPatchT backhoe ground truth data. This work was supported by the Air Force Research Laboratory under contract FA8650-04-1-1721.

REFERENCES

1. C. V. Jakowatz Jr., D. E. Wahl, P. H. Eichel, D. C. Ghiglia, and P. A. Thompson, *Spotlight-Mode Synthetic Aperture Radar: A Signal Processing Approach*, Kluwer Academic Publishers, Boston, 1996.
2. W. G. Carrara, R. S. Goodman, and R. M. Majewski, *Spotlight Synthetic Aperture Radar*, Artech House, Boston, 1995.
3. E. Rodriguez and J. Martin, "Theory and design of interferometric synthetic aperture radars," *IEE Proceedings F* **139**, pp. 147–159, Apr. 1992.
4. S. DeGraaf, "3-D fully polarimetric wide-angle superresolution-based SAR imaging," in *Thirteenth Annual Adaptive Sensor Array Processing Workshop (ASAP 2005)*, MIT Lincoln Laboratory, (Lexington, M.A.), 7 June – 8 June 2005.
5. C. D. Austin and R. L. Moses, "IFSAR processing for 3D target reconstruction," in *Algorithms for Synthetic Aperture Radar Imagery XII (Proc. SPIE 5808)*, SPIE Defense and Security Symposium, (Orlando, FL.), 28 March – 1 April 2005.
6. R. Bhalla and H. Ling, "Multi-baseline IFSAR study using an SBR based simulator," in *Algorithms for Synthetic Aperture Radar Imagery XII (Proc. SPIE 5808)*, SPIE Defense and Security Symposium, (Orlando, FL.), 28 March – 1 April 2005.
7. C. D. Austin, "Interferometric synthetic aperture radar height estimation with multiple scattering centers in a resolution cell," Master's thesis, The Ohio State University, 2006. (Available at `http://www.ece.osu.edu/~austinc`).
8. L. L. Scharf, *Statistical Signal Processing*, Addison-Wesley Publishing Company, 1991.
9. S. Kraut, L. L. Scharf, and R. W. Butler, "The adaptive coherence estimator: a uniformly most-powerful-invariant adaptive detection statistic," *IEEE Transactions on Signal Processing* **53**, pp. 427–438, Feb. 2005.